# RECONSTRUCTING HIGH-ACCURACY DEM WITH PRECISE ORBIT DATA AND EXTERNAL DEM

**A. Bin**

School of Marine Sciences
Sun Yat-sen University
Guangzhou 510275, China

**L. Xia**

School of Geography and Planning
Sun Yat-sen University
Guangzhou 510275, China

**X. Zheng**

Department of Electronic Engineering
Shanghai Jiao Tong University
Shanghai 200240, China

**Abstract**—Reconstructing high-accuracy Digital Elevation Model (DEM) is influenced by phase errors, such as phase trend, low coherence problems and phase unwrapping. These problems could result in the conversion errors from the phase to height. In this paper, a method is proposed to reconstruct the high-accuracy DEM using satellite interferometric synthetic aperture radar (InSAR). The proposed algorithm mainly aims to reduce the phase errors from the phase trend and low coherence problems. It consists of three steps. Firstly, the orbit state vectors are precisely interpolated in 3-D coordinates rather than in a separate dimension with the exploration of the orbital elements. Secondly, the relationship between external DEM and the interfermetric phase is built by the improved precise geo-location algorithm. The phase trend is estimated according to the topographic information and then removed from the unwrapped interferogram. Thirdly, the interferogram in low coherent regions are all updated with the simulated phases from actual DEM. The accuracy of the InSAR derived DEM can be significantly improved without any

ground control points (GCPs), especially in those regions contaminated by masses of residues. Meanwhile, the phase trend caused by atmosphere effects or orbits uncertainty can also be eliminated by using this method. The experiment has demonstrated the proposed method can yield quite satisfactory results for producing high-accuracy DEM using Envisat data.

## 1. INTRODUCTION

Interferometric synthetic aperture radar (InSAR) has been widely applied to digital elevation model (DEM) reconstruction or ground displacements researches related to a variety of processes, both natural and anthropogenic [1, 2]. In such applications, repeat-pass satellite modes, i.e., a single antenna observes the same area from different orbits with the same track, are mainly used in spaceborne interferometric techniques. These techniques are attractive for measuring and interpreting elevation information, motion or variations of the reflecting elements on the ground according to the phase differences between two SAR images [3, 4].

It is well considered that phase errors are one of the main error sources when reconstructing DEM by InSAR techniques [5]. The phase errors mainly consist of four parts: 1) phase trend in the interferogram; 2) errors caused by decorrelation and thermal noises; 3) atmospheric phase screen (APS) difference between master and slave images, which can be separated into the parts determined to topography or not [6, 7]; and 4) phase unwrapping process. These phase errors cannot be ignored in the reconstruction of high-accuracy DEM.

Although multi baseline synthetic aperture radar (SAR) interferometry can be exploited successfully for high-quality digital elevation model (DEM) reconstruction considering these errors [8, 9], it is complicated to combine the multi uncorrelated interferogram, and many scenes of images are required for the method.

Studies have indicated that the phase trend is mainly determined by the accuracy of orbit data (i.e., accurate baseline evaluation) [10, 11]. The parts of APS dependent on the topography are also related to orbit accuracies [7]. Therefore, accurate orbit data are crucial for DEM reconstruction.

Currently for European Space Agency (ESA) satellites ERS-1/2 and Envisat, Delft Institute of Earth-Oriented Space Research (DEOS) can provide highly precise orbits with a radial precision of 5–6 cm [10]. However, its available orbit data are sampled in a 1 second-interval, which requires an interpolation to meet a large number of azimuth data samples. And the error from the orbit data interpolation will

impact the accuracy of DEM reconstruction to some extent, assuming the spatial baseline of the interferogram shows 100 meters, the error of 0.5 meter for the orbit will result in about the error of 600 m in DEM reconstruction [21]. Conventional methods simply employ polynomial functions (e.g., second or higher order polynomial models) to fit all the orbit data provided in header file or obtained from DEOS in separate dimension. This is inaccurate due to its neglect of the orbit configuration. With the satellite's orbital elements well considered during orbit data interpolation, higher accuracy will be achieved for the further processing, and the phase trend due to the orbit error correspondingly will be greatly reduced.

Overall phase trends may result in elevation errors in unwrapped phase images. These errors may either be removed in the phase subtraction step by using the least squares fitting techniques to adjust the scaling of the reference phase images, or, be estimated with FFT flattening techniques [12]. The phase trends can be also reduced or removed by using the ground control points (GCPs). However, usually the GCPs are difficult to define in the interferogram especially in some areas such as steep mountains [7].

If there are no obvious geometric variations in the study area, external DEM can be directly used as reference data. Low-resolution shuttle radar topography mission (SRTM) data are generally used as external DEM in InSAR techniques. These data have been used to remove the topography phase in differential interferogram, to flat the interferogram, also to geocode the InSAR products, and so on [7, 12]. In this paper, the SRTM data are also selected as reference for retrieving simulated phase to match the interferogram. Then, phase trend in the unwrapped interferogram can be well modeled according to build the relationship between the simulated phase and interferogram facilitated by the more accurate precise orbit data.

On the other hand, low coherence problems are also caused by decorrelation during imaging interval. The phases within low coherent areas show disorganized patterns, which usually cause the phase unwrapping difficult and inaccurate. Although some assistant techniques such as stereoscopy [13] and clinometry [14] outside InSAR technique can be used to solve low coherence problems, it is generally difficult and complicated to make the results from these methods well matched with the unwrapped phase, more elaborated methods should be developed to recover the phases in low coherent area. If some external data can be directly used as a reference, it is expected that the phase errors in low coherent area will be more accurately removed.

This paper attempts to develop the methodologies to mainly solve the phase trend and low coherence problems for producing high-

accuracy DEM without any ground control points (GCPs). The main procedures are described in details in the following sections. An improved interpolation method for processing orbit data is introduced by revealing the satellite's orbital elements in 3-D coordinates rather than in separate dimension. The simulated phase is then retrieved by the improved precise geo-location algorithm to provide information for phase trend removal and low coherence problem solution. A subset scene of Envisat imaging from Bam, a city located in Kerman Province of Iran, is further selected as the sample area to validate this proposed method.

## 2. METHODOLOGY

### 2.1. Obtaining and Processing the Precise Orbit Data

The satellite orbit data refer to the satellite's instantaneous location (that is, XS, YS, and ZS) in the WGS84 coordinate system. In the data processing procedures, acquiring and processing satellite's precise orbits are crucial for further analyses, such as: 1) coarse co-registration of the image pair; 2) calculation of the reference phase on the ellipsoid; and 3) conversion of radar coded heights to geocoded coordinates. For a full SAR imaging scene, only several orbit data points with one second interval can be provided for all the azimuth lines. Therefore it is important to find an effective interpolation method to accurately obtain the position at every imaging location with the sample times provided by the precise orbit data. A polynomial fitting in separate dimensions is usually employed by using conventional methods. Although the satellite's location is relatively stable, such simple interpolation is rather inaccurate. In order to overcome this limitation, this paper presents an improved interpolation method by revealing the satellite's orbital elements from known 1s-interval orbit data. As it is done in the open source software DORIS, the conversion requires about 5 seconds before the first and after the last imaging time respectively to avoid the interpolation error in the image margin. The orbit data can be synchronously interpolated in 3-D coordinates rather than in a separate dimension.

It is well known that a satellite's instantaneous location is determined by six orbital elements shown in Table 1 [15].

The satellite's instantaneous location $(x(r),\ y(r),\ z(r))$ in the WGS84 coordinate system (i.e., the earth-rotated reference frame) is therefore computed by:

$$\begin{bmatrix} x(r) \\ y(r) \\ z(r) \end{bmatrix} = M_{H_G}^Z M_{-\Lambda}^Z M_{-i}^Z M_{-\omega}^Z \begin{bmatrix} r\cos\theta \\ r\sin\theta \\ 0 \end{bmatrix} \qquad (1)$$

**Table 1.** Orbital parameters.

| $a$ | $e$ | $i$ | $\Lambda$ | $\omega$ | $\tau$ |
|---|---|---|---|---|---|
| semi-major axis | the eccentricity | the orbital inclination | longitude of the ascending node | the orbit argument of perigee | time past ascending node |

where, $H_G$ is the Greenwich time for a vernal equinox, the satellite's range to the Earth's core $r$ and true anomaly $\theta$ are functions of $a$, $e$ and $\tau$ [15]. $M_\alpha^b$ indicates the rotation matrix of an angle $\alpha$ around an axis $b$.

Among all the six orbital elements, the first five parameters (corresponding to the orbit) can be obtained in the annotation data, leaving the last one varied. With the known 1s-interval time $t$ from DEOS, a polynomial function can be constructed for describing the dependence of $\tau$ on $t$. It will be further tested that a cubic polynomial is sufficient in accuracy. Then the satellite orbit data can be computed by Equation (1). Compared with the conventional methods, only the orbital element $\tau$ is interpolated for every azimuth time, the interpolation method synchronously interpolates the orbit data in 3-D coordinates rather than in separate dimensions. The orbital error can be restrained below 0.4 cm.

## 2.2. Forming the Relationship Between the Interferogram and the Simulated Phase

Studies have indicated that the phase trend is mainly caused by the orbital data errors [10, 11]. More accurate orbit data can be obtained according to the above procedures. The phase trend correspondingly can be significantly reduced in the unwrapped interferogram. However, no matter what interpolation method is used, the residual phase trend due to orbit errors will still remained in the unwrapped phase. As discussed above, the relationship between simulated phases and the actual unwrapped interferogram can be well built if the external reference DEM data can be obtained based on the achieved precise orbit data. Considering the feature of SRTM (Shuttle Radar Topography Mission), these data can be used as the reference for removing the residual phase trends. In this paper, an improved precise geolocation algorithm is introduced to build the relationship between the SRTM data and the unwrapped interferogram.

The SRTM equipped the Space Shuttle Endeavour with two

antennas during an 11-day mission in February 2000 and obtained elevation data on a near-global scale [16]. Nowadays the 1 arc-second (about 30 m) resolution data of the USA and 3 arc-second (about 90 m) resolution data of other area regions have been available for public use. These data have horizontal and vertical accuracy near 20 m and 16 m respectively (linear error at 90% confidence) [17].

Based on the satellite orbit data in each azimuth time, it is convenient to transform the SRTM DEM to radar coordinates. These coordinates can then be easily interpolated to integer coordinates (re-gridding). Some researches showed this can be done with the nearest neighbor method [18]. However, this method may have the following problems:

- It is difficult to construct a one-to-one correspondence between the raw interferogram and the DEM, especially for the boundary of the imaging area.
- Only the size of the DEM, and not the size of the interferogram, affects the numerical cost. This is inefficient for dealing with large areas [19].

An alternative simulation method, that is, the precise geo-location algorithm was then adopted by some researchers to solve the above problems [12]. The proposed method works from an interferogram pixel, and then finds its corresponding SRTM DEM (both height and location) by interactively solving according to the following Equations (2)–(4):

$$(\mathbf{S}_1(\tau) - \mathbf{P}) \cdot \dot{\mathbf{S}}_1(\tau) = 0 \tag{2}$$

$$|\mathbf{S}_1 - \mathbf{P}| = r_1(t) \tag{3}$$

$$\frac{P_x^2 + P_y^2}{(a + h)^2} + \frac{P_z^2}{(b + h)^2} = 1 \tag{4}$$

where $\mathbf{S}_1(\tau)$ and $\dot{\mathbf{S}}_1(\tau)$ represent the master antenna's location and velocity as a function of the SAR azimuth time $\tau$ respectively, $P(P_x, P_y, P_z)$ is a target's position in the WGS84 coordinate system, and $\lambda$ is the radar wavelength; $r_1(t)$ is the range between the master antenna and the target $\mathbf{P}$ also as a function of the SAR range time $t$. The Earth semi-major $a$ and semi-minor axis $b$ have been modified by the target $\mathbf{P}$'s height $h$.

Once a tentative $\mathbf{P}$ with the location and height has been determined, a table search is carried out in the SRTM data. The actual terrain's height for an interferogram sample can be determined if this height with the same location in SRTM DEM is equal, or sufficiently approximate to $h$; Otherwise procedures of (2)–(4) are repeated. Then

the zero-Doppler position of the slave antenna is determined according to the following equation:

$$(\mathbf{S}_2(\tau) - \mathbf{P}) \cdot \dot{\mathbf{S}}_2(\tau) = 0 \tag{5}$$

Finally, the range difference between the ground point and the two antennas provides the interferometric phase $\varphi$ by:

$$\varphi = -\frac{4\pi}{\lambda} \left( |\mathbf{S}_1(\tau) - \mathbf{P}| - |\mathbf{S}_2(\tau) - \mathbf{P}| \right) \tag{6}$$

Although the above procedures seem to provide better effects, there are still some other technical issues which should be addressed:

1) DEM interpolation: the resolution (about 90 m) of SRTM DEM is well below that of the interferogram. To make the relationship between the DEM and the interferogram more precise, the DEM has to be interpolated, and correspondingly, the interferogram has to be multilooked to achieve an eclectic resolution (e.g., 40 m).

2) Obtaining the target's position: a closed-form expression of $P(P_x, P_y, P_z)$ is unobtainable from (2)–(4), so the Newton's iteration method is used, starting at geographic coordinates of the scene centre given in the annotation data. This is true for (5) as well. Normally, after 3 or 4 iterations, the solution converges to values better than $10^{-6}$ m and $10^{-10}$ s, respectively [12].

3) Building the 3-D geometry approximation to save running time: the coordinate transformations within the iteration loop on every pixel point make the computation quite slow [19], only parts of pixels were determined with the Newton's iteration, and then the polynomial interpolation was used both in height and the geometry. As geo-location of every pixel in the image scene varies slowly with the height, a cubic polynomial is sufficient to model this relationship (1-D approximation). Meanwhile, the SAR imaging geometry changes slowly in range and azimuth [19] and can, also approximately expressed by introducing a grid on the interferometric data (2-D approximation). A significant acceleration is achieved by using both 1-D and 2-D approximation above.

4) Obtaining the height derived from DEM: the bisection algorithm, instead of point-wise search, is used to find the height in DEM range. However, if there is either layover or shadow effects, more than one root exist, and the actual point is not directly calculated but interpolated from the neighbors.

Hence, the simulated phase corresponding to each interferometric pixel can be computed by Equation (6). The phase trend can then be more accurately removed by comparing the relationship between the actual interferogram and the simulated one. This procedure is further discussed in the following section.

## 2.3. Removing the Phase Trend Based on the Simulated Interferogram

The actual interferogram consists of the following parts [3]:

$\phi_r$: Sensor-target range difference between sensors;

$\phi_t$: Possible physical and geometric character changes of ground scatters;

$\phi_a$: Changes of atmosphere between two data acquire times;

$\phi_n$: Thermal noise etc;

Then the intereferogram phase can be correspondingly denoted as follows:

$$\phi = \phi_r + \phi_t + \phi_a + \phi_n \tag{7}$$

wherein, $\phi_r$ can be generally divided into two parts: the phase related to the topographic information $\phi_z$, and the 'flat earth phase' $\phi_{flat}$ caused by orbit respectively. The topographic information $\phi_z$ is aimed to obtain accurately with InSAR technique in this paper. $\phi_t$ can be ignored if the time interval between the two imaged scenes is small, especially during the time where no seriously geographic variation such as earthquake appeared in the urban area. However, $\phi_a$ is very complicated, which can also be separated as the parts determined to topography or not. $\phi_n$ is mainly due to the imaging system, which can be neglected in regression analysis for large number of regression samples [7]. Then, the obvious phase trend due to the orbit errors will be exposed to the unwrapped interferogram. In this paper, the phase trend is modeled and then removed according to the relationship between the simulated phase from external SRTM data and the unwrapped interferogram.

Firstly, the topography information derived from the SRTM should be assumed to be the same as actual DEM. This is also further validated with the results from DORIS software. Then, the phase derived from external DEM can be used as reference to evaluate the quality of removing the phase trend. Comparing the actual unwrapped interferogram with the simulated phase, the phase trend can be expressed by using the following linear model considering the atmospheric influence [7]:

$$\phi_{trd} = c + l_1 i + l_2 j + l_3 \phi_z \tag{8}$$

where, $i$ and $j$ represents the row and the column respectively, $\phi_z$ is the phase which is only related to the height above sea level derived from the SRTM data, and $l_1$, $l_2$ is the slope of phase trends along the azimuth and slant range directions, $l_3$ denotes the influence coefficient of topographic information.

The phase trend varies slowly both in azimuth and slant direction, linear model can basically meet the phase accuracy. In this paper, this

linear method is firstly used to evaluate phase trend $\phi_{trd}$. However, such linear method may have limitations because usually, there is complex relationship between phase trends and the topographic information $\phi_z$. It is also considered that parts of the phase errors due to APS depend on topography [7], and the polynomial function can be built between them. A solution to capture such complex relationship is to use polynomial models for evaluating phase trend. It is expected that polynomial models may provide better performance. In this paper, several polynomial functions will be tested for phase trend simulation so that better performance can be achieved. The polynomial model is based on the quadratic and cubic equations:

$$\phi_{trd} = f(i, j, \phi_z) = \sum_{m=0}^{d} \sum_{n=0}^{d} \sum_{k=0}^{d} l_{m-n,n-k,k} i^{m-n} j^{n-k} \phi_z^k \qquad (9)$$

where $d$ is 2 or 3.

## 2.4. Replacing the Interferometric Fringes within the Low Coherent Area with Simulated Values

In the repeat-pass modes, decorrelation for non-simultaneous imaging acquisition will bring a lot of noises in the interferogram and useful information tends to be overshaded [20]. This will make it difficult for phase unwrapping. Within the low coherent area, the phase information deviates from the actual value and varies irregular, the unwrapped phase is significantly different from the actual height elevation. This will then result in higher errors for reconstructing DEM. Therefore, the low coherence problem will be further tackled. The process mainly includes: 1) updating interferogram phases in low coherent areas with simulated ones; 2) phase filtering and unwrapping; 3) phase trend removal.

As described, the simulated phase derived from actual DEM is well related to the interferogram, which can then be taken as accurate reference phase. According to the Section 2.3, the simulated phase is well matched with the interferogram, and if the low coherent area is defined, then phases within these areas can be directly updated by the simulated ones. This will provide valuable interferometric information for phase filtering and unwrapping in the low coherent area.

A minimum cost flow (MCF) unwrapping method will be used in this paper, based on the updated interferogram, residue density, average scene coherence, mean scene height and mean scene height variation should be produced, and then positive and negative residues are paired and connected by a line segment [22]. It is regarded that, the phase inconsistency is caused when the integration path crosses

the line segment. The optimized line segment will be achieved with the coherence as cost value. It is expected to significantly reduce the residues influence (phase singular points) on the interferogram with the substitution of simulated phase in the low coherent area. Then the phase trend is removed from the unwrapped interferogram with the polynomial Equation (9).

Here, the coherence value of 0.45 is used as threshold for distinguishing the low coherent area, and the substitution with the simulated DEM phase is carried out in the extend area with the minimum size of 5 pixels. The accuracy of derived DEM within the low coherent region by using this proposed method is close to that of SRTM. However, the derived DEM can have a higher spatial spacing than that of SRTM.

## 3. IMPLEMENTATION RESULTS AND DISCUSSION

A part of Bam scene in Iran is selected as an example, which was respectively imaged by Envisat ASAR on June 11th and December 3rd, 2003. The satellite's flight time elapses about 16 seconds, there are almost 27000 lines (i.e., azimuth time) of data for the whole scene. The proposed method is used to remove the phase trend and solve low coherence problem for high-accuracy DEM reconstruction.

The orbit data are processed with the proposed interpolation method. The experiments have indicated that a cubic polynomial is sufficient in terms of accuracy. To validate the efficiency of the interpolation method, a simple and efficient method is then used to compare the improved method with a conventional one. Orbital data was decimated into two groups, odd seconds and even seconds, odd seconds is selected as samples to acquire polynomial coefficients, and even seconds are accordingly used to verify the models' efficiency. The results are shown in Table 2, which indicates a better orbit accuracy of about 1 cm (corresponding to 6m height accuracy) by this interpolation method.

Then, the simulated phase is derived from external SRTM data for removing the phase trend. Figure 1 is about the coherence map, raw interferogram and simulated interferogram based on SRTM. The

**Table 2.** Error comparison of interpolation method.

|  | Max error (cm) | Mean error (cm) |
| --- | --- | --- |
| Conventional method | 1.212 | 0.703 |
| Our method | 0.319 | 0.087 |

unwrapped phase of simulated interferogram and actual flattened interferogram (interferogram with flat earth phase removed) are shown in Figures 2(a) and Figure 2(b) respectively.

It is easy to find that, there is a difference between the actual interferogram and the simulated one. And from the coherence map, several low coherent areas are also obviously displayed. Especially, the phases are more fragmented with noises in the raw interferogram.

A further step is to subtract the topography phase $\phi_z$, which is shown in Figure 3(a). The phase trends clearly show some correlation with the topography. The linear model as Equation (8) is then used to compute and remove the phase trend from the actual unwrapped



(a)                           (b)                           (c)
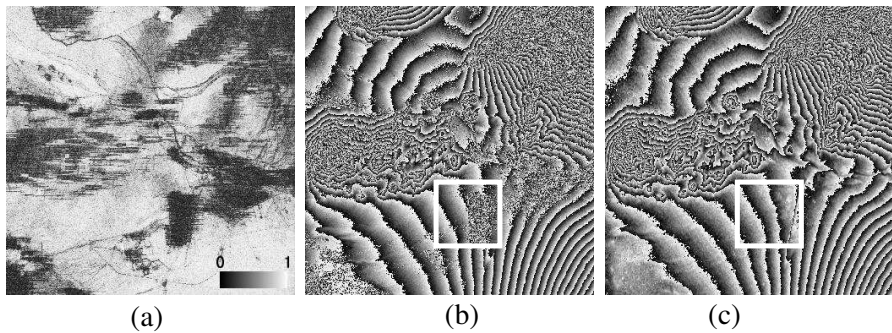
**Figure 1.** Coherence map, raw Interferogram and simulated interferogram based on SRTM. (a) Coherence Map (ranging from 0 to 1). (b) Raw interferogram. (c) Simulated interferogram.



(a) Unwrapped Phase Derived from SRTM

(b) Unwrapped Interferogram with flat earth phase removed
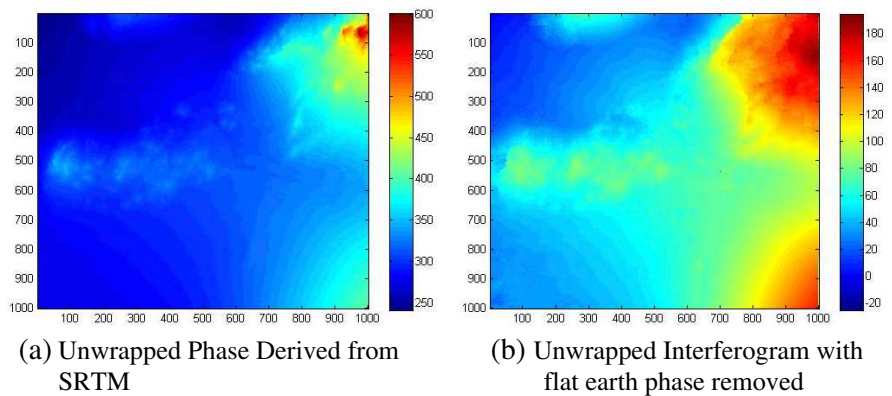
**Figure 2.** Unwrapped phase: (a) simulated phase; (b) unwrapped interferogram with flat earth phase removed.
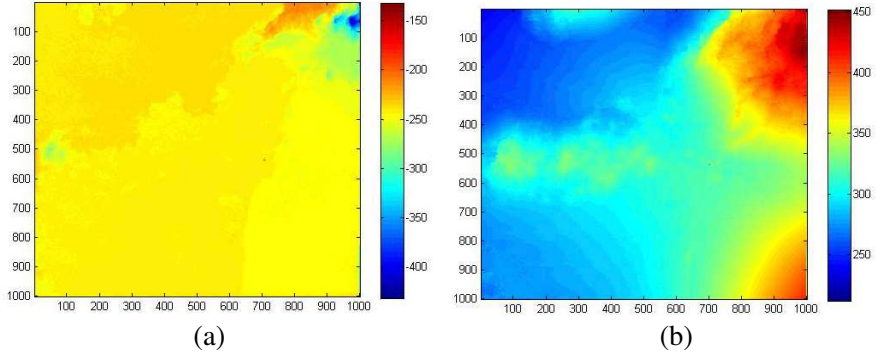
**Figure 3.** (a) Difference between the original unwrapped phase and simulated phase; (b) phase trend removed with the linear method.
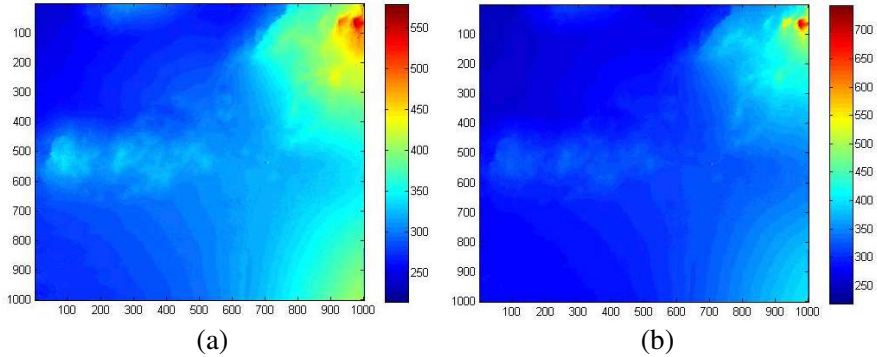


**Figure 4.** Phase trend removed with polynomial models: (a) phase trend removed with quadratic model; (b) phase trend removed with cubic model.

interferogram. The result is shown in Figure 3(b).

It is easily found that, the whole pattern of the unwrapped interferogram with phase trend removed is similar with the unwrapped raw interferogram as shown in Figure 2(b). This shows that residual phase trend is still remained in the unwrapped interferogram, the linear simulation model cannot produce satisfactory accuracy. The polynomial model as Equation (9) is further validated. Results are shown in Figure 4.

It can be noted that the phase map is quite different from the raw interferogram if the phase trend simulated with polynomial model is not included (shown as Figure 4(a) and Figure 4(b)). The phase pattern is more close to that simulated from external reference DEM.
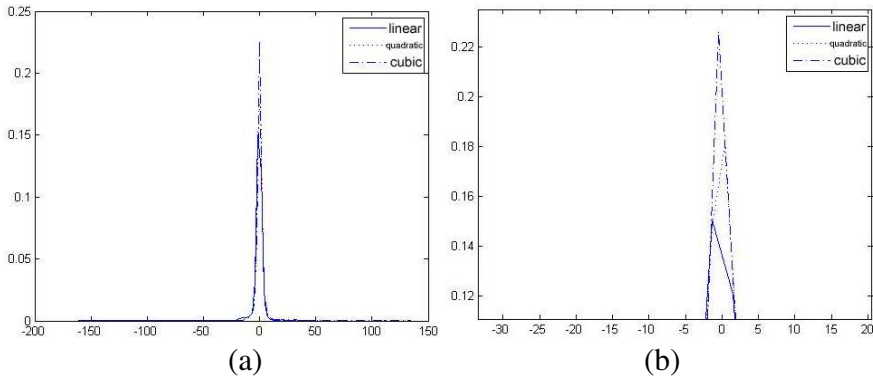
**Figure 5.** Pattern of models' errors probability: (a) the whole pattern of models' errors probability; (b) local zooming of (a) (Horizontal axe represents the value of errors, and the vertical axe expresses the probability of some error).

**Table 3.** Means and standard deviations of the linear and polynomial models' errors.

|  | Linear model | Quadratic model | Cubic model |
|---|---|---|---|
| Mean (deg) | −38.9097 | −5.4964 | 5.2051 |
| Std. (deg) | 34.1474 | 20.8522 | 22.8709 |

The probability, the means and standard deviations of models' errors are calculated for validating the results. The validations are shown in Figure 5 and Table 3.

The models' errors probability (Figure 5(b)) shows that the polynomial model has a low simulation error for phase trend removal. Moreover, the errors from the quadratic model are very close to those from the cubic model.

Table 3 indicates that the mean and standard deviations of simulation errors from the polynomial model are obviously lower than those of the linear model. Especially the mean error can be well controlled to a lower level for the polynomial model. Table 3 and Figure 5 indicate that the quadratic model seems to be the best option for modeling phase trends. Phase error due to parts of APS dependent on topography can be synchronously removed with the nonlinear simulation model. However, because the phase error from APS independent on topography is random and more complex, it is difficult to remove by using this simple method.

The polynomial model still has a high value of the standard
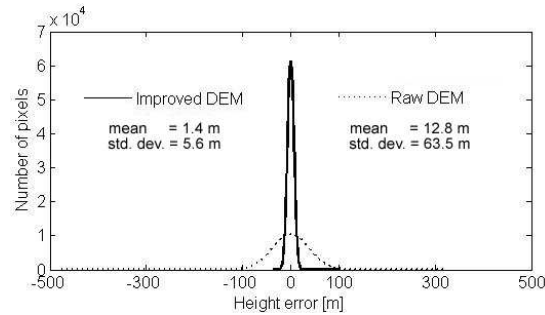
**Figure 6.** Histogram of different DEM height error.

variations (Table 3), although it can yield a relatively lower value. Actually, it is easily understood from the coherence map (Figure 1(a)), parts of which shows lower value due to decorrelation for non-simultaneous imaging acquisition.

The rectangular region listed in Figure 1(b) and Figure 1(c) shows low values in the coherence map (Figure 1(a)), and where the phases are correspondingly disorganized in the raw interferogram map (Figure 1(b)). The area is then further focused to explain the solution for low coherence problems. With a topographic map obtained from survey department as a reference, the height values between the reference DEM and that derived in this paper are compared with the point to point analysis, the patterns of height errors (i.e., accuracy of DEM reconstruction) shown as Figure 6, the relationship between the height error and coherence value shown as Figure 7 are further analyzed for validating the results.

Where raw DEM refers to that derived from unwrapped interferogram only with phase trend removed, while improved DEM represents that derived from raw one with phases in low coherent area further substituted.

It can be found that, height errors of raw DEM vary from $-100\,\mathrm{m}$ to $100\,\mathrm{m}$. The mean value and standard deviation are $12.8\,\mathrm{m}$ and $63.5\,\mathrm{m}$ respectively. The overall accuracy of DEM reconstructed is relative lower. However, on the contrary, the histogram of improved DEM shows a peak around zero, the mean and standard deviation are reduced to $1.4\,\mathrm{m}$ and $5.6\,\mathrm{m}$ respectively. This method can yield a higher accuracy of DEM reconstruction.

According to the relationship between coherence values and height errors in Figure 7, it can be found that the higher height errors of raw DEM mainly centralize around the lower coherent area, especially when coherence values are lower than 0.2. However, the height
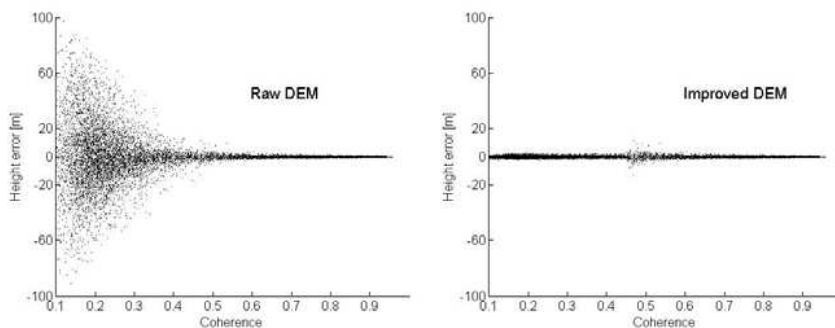
**Figure 7.** Derived height error versus interferometric coherence in the rectangle of Figure 1(b) and Figure 1(c), respectively.

errors of improved DEM scatter nearby zero including low coherent area. The experiments indicate that the higher-accuracy DEM can be reconstructed if low coherence problems have been solved.

## 4. CONCLUSION

During reconstructing high-accuracy DEM, phase errors caused by different sources usually result in inaccurate unwrapped phase. This paper attempts to develop the methodologies for reducing the errors caused by phase trends and low coherence problems to reconstruct high-accuracy DEM based on precise orbit data and external DEM. The method mainly includes the following procedures: 1) obtaining and interpolating the precise orbit data with an improved method; 2) building the relationship between the interferogram and the external reference DEM more accurately with InSAR geometry; 3) modeling and removing the phase trend; and 4) recovering the phases in low coherent area by using the simulated phases.

As the phase trend is mainly due to the orbital errors, the improved interpolation method based on the satellite's orbital elements is introduced to retrieve high-accuracy orbit data in 3-D coordinates rather than in a separate dimension. This method can achieve a better accuracy of about 1 cm (corresponding to 6 m height accuracy) for orbit data.

The simulated phase derived from external reference SRTM data by using this improved precise geo-location algorithm can then be well matched to the interferogram with the InSAR geometry according to the interpolated orbit data. This can provide efficient information for removing phase trends from the unwrapped interferogram and

solving low coherence problems. High-accuracy DEM can then be reconstructed even without any ground control points (GCPs).

This study has tested three different simulation models by using sample data. The phases in low coherent area are further replaced by using simulated ones. Experiments indicate that the quadric model has a lower error. It is more adaptive for the phase trend removal than the conventional linear model. The derived DEM can have higher spatial spacing than SRTM within low coherent areas, although the accuracy is approximated to that of SRTM.

## ACKNOWLEDGMENT

## REFERENCES

1. Massonet, D. and K. L. Feigl, "Radar interferometry and its application to changes in the earth's surface," *Reviews of Geophysics*, Vol. 36, No. 4, 441–500, 1998.

2. Rosen, P. A., S. Hensley, and I. R. Joughin, "Synthetic aperture radar interferometry," *Proceedings of the IEEE*, Vol. 88, 333–382, 2000.

3. Hanssen, R. F., *Radar Interferometry Data Interpretation and Error Analysis*, 63–64, Kluwer Academic Publishers, Dordrecht, 2001.

4. Wang, C., H. Zhang, and Z. Liu, *Space-born Synthetic Apture Radar Interferometry,* 48–49, Science Press, Beijing, 2002.

5. Zebker, H. A. and R. M. Goldstein, "Topographic mapping from interferometric synthetic aperture radar observations," *Journal of Geophysical Research*, Vol. 91, No. B5, 4993–4999, 1986.

6. Goldstein, R., "Atmospheric limitations to repeat-pass interferometry," *Geophysical Research Letters*, Vol. 22, No. 18, 2517–2520, 1995.

7. Liao, M. S., T. Wang, and L. J. Lu, "Reconstruction of DEMs from ERS-1/2 tandem data in mountainous area facilitated by SRTM data," *IEEE Transactions on Geoscience and Remote Sensing*, Vol. 45, No. 7, 2325–2335, 2007.

8. Ferretti, A., C. Prati, and F. Rocca, "Multibaseline InSAR DEM

reconstruction: The wavelet approach," *IEEE Transactions on Geoscience and Remote Sensing*, Vol. 37, No. 2, 705–715, 1999.

9.  Li, J., H. F. Huang, and D. N. Liang, "A multi-baseline InSAR DEM reconstruction approach without ground control points," *Proceeding of the 2007 International Geoscience and Remote Sensing Symposium, IGARSS' 2007*, 4509–4512, 2007.

10. Scharroo, R. and P. Visser, "Precise orbit determination and gravity field improvement for the ERS satellites," *Journal of Geophysical Research*, Vol. 103, No. C4, 8113–8127, 1998.

11. Chen, Q., G. X. Liu, and Y. S. Li, "Comparison and evaluation on accuracy in satellite InSAR DEM derived using coarse and precise orbit data," *Journal of Remote Sensing*, No. 10, 475–480, 2006 (in Chinese).

12. Geudtner, D. and M. Schwäbisch, "An algorithm for precise reconstruction of InSAR imaging geometry: Application to "flat Earth" phase removal, phase-to-height conversion, and geocoding of InSAR-derived DEMs," *Proceeding of EUSAR'96*, 249–252, Könogswinter, Germany, 1996.

13. Gelautz, M., P. Paillou, C. W. Chen, and H. A. Zebker, "Radar stereo-and interferometry-derived digital elevation models comparison and combination using Radarsat and ERS-2 imagery," *International Journal of Remote Sensing*, Vol. 24, No. 24, 5243–5264, 2003.

14. Guarino, C., "SAR interferometry: A novel method for enhancing elevation maps by combining interferometry with shape-from-shading," *IEEE International Conference on Image Processing*, No. 1, 45–48, 1996.

15. Montenbruck, O. and E. Gill, *Satellite Orbits — Models Methods Applications*, Springer, Berlin, Heidelberg, New York, 2000.

16. Jet Propulsion Laboratory, "Shuttle radar topography mission: Mission overview," Available online at: http://www2.jpl.nasa.gov /srtm/missionoverview.html, Aug. 28, 2005.

17. Smith, B. and D. Sandwell, "Accuracy and resolution of shuttle radar topography mission data," *Geophysical Research Letters*, Vol. 30, No. 9, 1467–1470, 2003.

18. Goblirsch, W., "The exact solution of the imaging equations for crosstrack interferometers," *Proceeding of the 1997 International Geoscience and Remote Sensing Symposium (IGARSS' 97)*, No. 1, 439–441, 1997.

19. Eineder, M., "Efficient simulation of SAR interferograms of large areas and of rugged terrain," *IEEE Transactions on Geoscience*

*and Remote Sensing*, Vol. 41, No. 6, 1415–1427, 2003.

20. Zebker, H. A. and J. Villasenor, "Decorrelation in interferometric radar echoes," *IEEE Transactions on Geoscience and Remote Sensing,* Vol. 30, No. 5, 950–959, 1992.

21. Xiang, Z. and X. Z. Liu, "Analysis of the InSAR flattening errors and their influence on DEM reconstruction," *IEEE Radar Conference*, Vol. 4976989, May 2009.

22. Suchandt, S. and M. Eineder, "Experiences with SRTM/XSAR phase unwrapping using the minimum cost flow method," *Proceeding of IEEE International Geoscience and Remote Sensing Symposium*, Toulouse, 2003.